



Characterization of geothermal water in the piedmont region of Qinling Mountains and Lantian-Bahe Group in Guanzhong Basin, China

Panpan Xu^{1,2} · Qiyang Zhang^{1,2} · Hui Qian^{1,2} · Mengna Li^{1,2} · Kai Hou^{1,2}

Received: 26 February 2019 / Accepted: 7 July 2019 / Published online: 19 July 2019
© Springer-Verlag GmbH Germany, part of Springer Nature 2019

Abstract

The piedmont region in the Qinling Mountains (QL) is a recharge area for geothermal water in the Guanzhong Basin, and the Lantian-Bahe Group (LB) is the main mining layer for the geothermal water in the basin. This study focuses on the origin, classification and reservoir conditions of geothermal water in the QL and LB by combining geochemical and isotopic approaches and principal components analysis (PCA). QL water types are $\text{HCO}_3\text{-SO}_4\text{-Ca-Na}$, $\text{HCO}_3\text{-SO}_4\text{-Na-Ca}$ and $\text{SO}_4\text{-HCO}_3\text{-Na}$, while $\text{SO}_4\text{-Cl-Na}$ and Cl-Na are major types in BL. QL geothermal water is a cycling-type water and it receives a large amount of meteoric water in an open reservoir environment. The main and secondary sources of QL geothermal waters are modern infiltration water and ancient lexiviation water, respectively. LB geothermal water originates from ancient lexiviation water, modern infiltration water and residual sedimentary water in a semi-closed or closed reservoir environment. Both of these geothermal water bodies have a direct or indirect hydraulic connection with faults. The formation of QL geothermal water is dominated by vertical heat conduction, followed by horizontal convection, and the main geothermal formation model of the LB is vertical heat conduction. The obtained values are 20.3–97.6 °C and 75.7–116.6 °C for QL and LB, respectively, indicating low–medium temperature fluids.

Keywords Geothermal water · Isotope and hydrochemistry · Principal component analysis · Geothermometer · Qinling Mountains

Introduction

Geothermal resources, as one of the possible clean energy sources, are used in many countries including Turkey (Davraz et al. 2017), Germany (Baumann et al. 2017), Spain (Blasco et al. 2017), China (Zhu et al. 2018), Mexico (Pinti et al. 2017), and USA (Etzzel et al. 2017). Judging by the

increasing development trends in this industry, the large-scale exploitation and utilization of geothermal energy may become very popular. Geothermal water is extensively used in industrial processing, geothermal heating, hot spring bathing, rehabilitation medical treatments, planting and breeding, etc., and provides a certain degree of economic, social and environmental benefits.

Large river basins host a huge population and are the origin of human civilization. Human activities in large river basins are extensive and intensive, which have caused various environmental issues (Li et al. 2014a, b, 2017; Wu and Sun 2016; Zhang et al. 2018). Particularly, the consumption of fossil energy such as coal and petroleum for industrial and domestic purposes and irrational water resources development has produced serious air pollution, water contamination and soil quality degradation (Li and Wu 2019; Li et al. 2018a, b). China with no exception is facing many environmental problems. To address the environmental issues in human-concentrated basins caused by the consumption of fossil energy, geothermal resources have been widely

This article is a part of the Topical Collection in Environmental Earth Sciences on “Water in Large Basins” guest edited by Peiyue Li and Jianhua Wu.

✉ Hui Qian
qianhui@chd.edu.cn

¹ School of Environmental Science and Engineering, Chang’an University, No. 126 Yanta Road, Xi’an 710054, Shaanxi, China

² Key Laboratory of Subsurface Hydrology and Ecological Effects in Arid Region of the Ministry of Education, Chang’an University, No. 126 Yanta Road, Xi’an 710054, Shaanxi, China

explored in these past few years in China. Geothermal resources of the Guanzhong Basin in Shaanxi Province are abundant and have been exploited on a fairly broad scale for more than 1000 years (Qin et al. 2005b). Thus, analysis of geological structure, hydrogeochemical environment and recharge sources can provide a scientific basis to research geothermal systems in the Guanzhong Basin. Numerous studies exist on hydrochemistry and environmental isotope evolution, characteristics of geothermal waters in this region, and they focus on occurrence forms, recharge–flow–discharge conditions and water–rock interactions (Ma et al. 2017; Qin et al. 2005a, b; Zhang 2016). It is worth mentioning that the piedmont of the Qinling Mountains is one of the most important sources for geothermal water in the Guanzhong Basin (Qin et al. 2005a), and it is also an important conservation area for geothermal water (Zhang 2016). Hence, systematic characterization of the geothermal fluids in the piedmont of the Qinling Mountains can provide guidance for sustainable development, utilization and protection of the geothermal water in the Guanzhong Basin. Despite the well-known interest in this geothermal system, its momentous supply area (the piedmont of the Qinling Mountains) is still poorly known due to the lack of comprehensive analysis on hydrological and hydrochemical features.

Multivariate statistical techniques, like principal components analysis (PCA), factor analysis (FA) and discriminant analysis (DA), are typically used to summarize water quality data (Dassi 2011; Li et al. 2013, 2019a; Wu et al. 2014, 2019; Zhang et al. 2014, 2016). These methods analyze the physicochemical characteristics of groundwater and hydrogeochemical processes and assess water quality (Duan et al. 2016; Qian and Li 2011; Zhang et al. 2014; Li et al. 2018c, 2019b). The PCA method converts multiple factors into a small number of mutually independent factors through linear changes, which improves the resolution of water quality information. PCA was used to identify hydrochemical processes occurring in the hydrothermal systems (Zhang et al. 2016). However, in some situations, usage of only multivariate statistical methods is not completely objective and credible. Hence, a combination of multivariate statistical approaches and hydrogeochemical methods plays a key role in identifying the water–rock interactions in geothermal systems.

Considering the weakness in previous research regarding the understanding of the recharge and occurrence of geothermal resources in the Guanzhong basin and the effectiveness of hydrochemistry and multivariate techniques in geothermal water studies, this study attempts to reveal recharge sources, water–rock interactions and origin types by combining the geothermal water in the piedmont of the Qinling Mountains and the center of Guanzhong Basin to enrich the study of the geothermal reservoir of the Qinling Mountains piedmont in the light of hydrogeochemical methods and PCA.

Site description

Geography and climate

The Guanzhong Basin is located in the middle of Shaanxi Province between 106°30' and 110°30'E, 33°00' and 35°20'N. It covers an area of ~20 thousand km². Its average elevation is about 400 m a.s.l.. The Qinling Mountains are on the southern edge of the basin spreading 1500 km in the east–west direction and 100–150 km in the north–south direction. Their elevation is around 500–2500 m a.s.l. (Fig. 1). The study area is characterized by warm temperate semi-humid continental monsoon climate. The average annual precipitation in the Guanzhong Basin and the Northern piedmont of Qinling Mountains is 550–750 mm and 850–1000 mm, respectively. 45–55% of the annual precipitation is concentrated in July, August and September (Zhang 2016). The average annual temperature is 13.1 °C. As the largest tributary of the Yellow River, the Wei River is 502.4 km long and has 538 million m³ of the average annual runoff in Shaanxi Province.

Geomorphological setting

In this region, the terrain from the piedmont to the center of the basin starts with the Qinling Mountains, then the piedmont alluvial fan, the loess plateau and the valley terrace (Fig. 1). The Qinling Mountains are mainly composed of metamorphic rocks of the Mesoproterozoic Erathem Kuanping Group. The piedmont alluvial fan is in the form of alluvial fan skirt or piedmont alluvial plain, exhibiting the characteristics of coarse granules of thick diluvial deposits. Two stages of the loess plateau were formed on the basis of the lower Pleistocene lake basin and at the end of the Tertiary period, respectively. The terraces of the Wei River Valley gradually become broad from west to east (Xu 2014).

Geologic and hydrogeological setting

The major structures in the study area are E–W and NE–SW stretching faults, which serve as the discharge channels for the upward flow of the geothermal fluids based on the distribution of the geothermal springs (Guo and Wang 2012; Ma et al. 2017) (Fig. 1). The faults stretching in a generally E–W direction are the Qinling North Piedmont fault, the Yuxia-Tieluzi fault and the Weihe fault. The Chang'an-Lintong fault consists of three parallel fractures and stretches in a NE–SW direction (Zhao 2009).

In this study area, the geothermal reservoirs are generally divided into two types: Qinling piedmont structure break crevasse geothermal reservoir (QPR) and Cenozoic

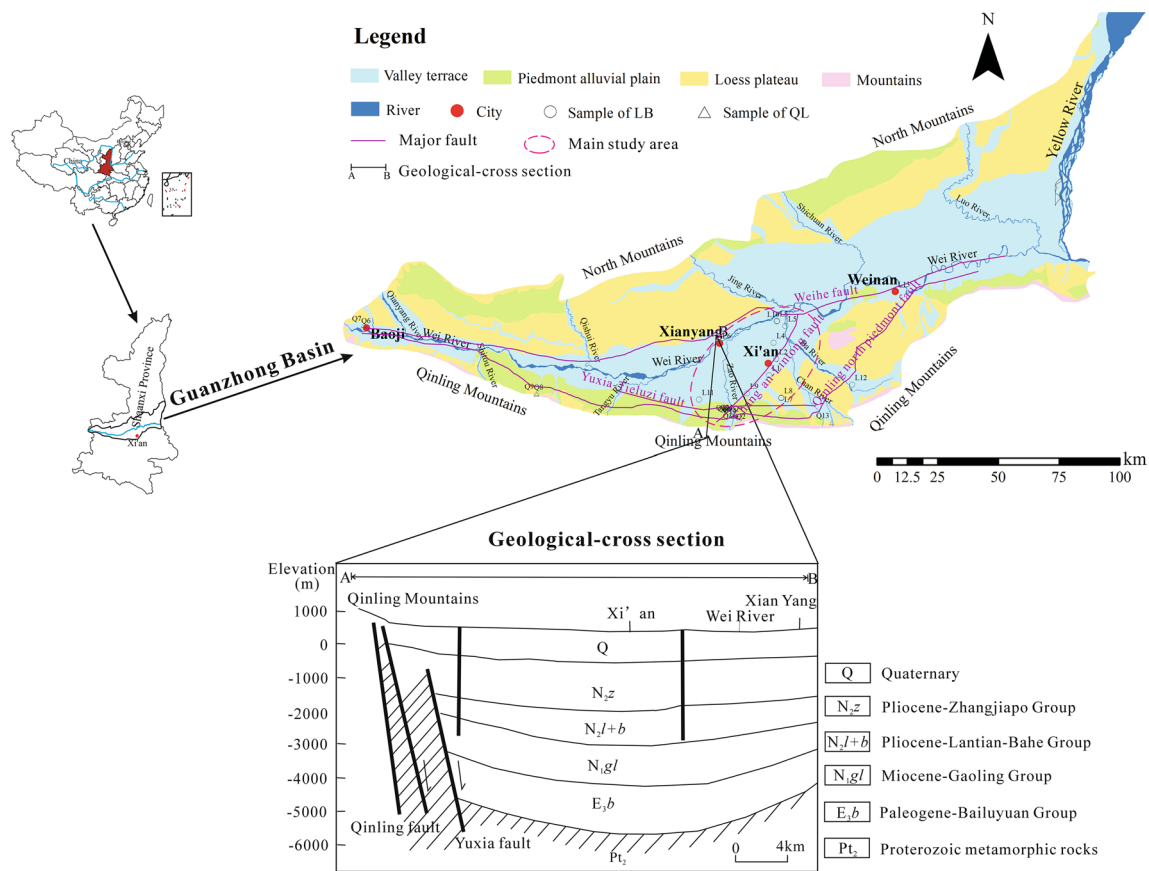


Fig. 1 Simplified geological map of the study area with sampling locations Compiled from: Ma et al. (2017)

sandstone–glutenite pore geothermal reservoir (CSR). The QPR is located along the Qinling fault in the south of the basin. Its geothermal wells are generally less than 1000 m deep and temperatures of geothermal water range from 30 to 60 °C. CSR can be subdivided into four sections [the Zhangjiapo Group (N₂z), the Lantian-Bahe Group (N₂l + b), the Gaoling Group (N₁gl), and the Bailuyuan Group (E₃b)] from top to bottom (Fig. 1). The Lantian-Bahe Group is currently the main thermal reservoir for development and utilization of the basin (Ma et al. 2017). Hence, the water samples of the central basin were collected from the Lantian-Bahe Group.

According to the AB geological-cross section in Fig. 1, the Quaternary (Q) sediments are situated at the top of the stratum and almost distribute throughout the Guanzhong Basin. The lithology is dominated by loess and gravel. Its reservoir has the geothermal temperatures of 30–50 °C and depths of 300–700 m (Xu et al. 2019). The Zhangjiapo Group (N₂z) belongs to yellow lime and gray-green fluvial and lacustrine facies strata with interbedded mudstone, sandy mudstone and sandstone (Mu et al. 2016). Its geothermal temperatures and depths are 40–70 °C and 500–1300 m, respectively (Xu et al. 2019).

The Lantian-Bahe Group (N₂l + b) is dominated by fluvial deposits, and its lithology is interbedded with gray-yellow and gray-white sandy conglomerate, mudstone and shale (Mu et al. 2016). The Lantian-Bahe Group is the main thermal reservoir in the center of the Guanzhong Basin with the geothermal temperatures and depths of 50–90 °C and 900–1800 m, respectively (Mu et al. 2016). The Gaoling Group (N₁gl) is a lacustrine deposit-dominated stratum with purple mudstone and thin siltstone, and it has the range of geothermal temperatures and depths of 80–120 °C and 1500–2400 m (Mu et al. 2016; Xu et al. 2019). The Bailuyuan Group (E₃b) is a fluvial–lacustrine sedimentary stratum with dark purple, gray-yellow mudstone interbedded with gray-white medium-fine sandstone and coarse sandstone. Its geothermal temperatures and depths range from 130 to 150 °C and from 2900 to 3100 m, respectively (Mu et al. 2016). The Proterozoic metamorphic rocks (Pt₂) are located mainly within the Qinling North Piedmont fault zone (Xu et al. 2019). The minerals of the reservoir rocks in the study area mainly contain analcite, Na-feldspar, calcite, quartz, fluorite, muscovite, chalcedony, anhydrite, and chrysotile (Qin et al. 2005b).

Materials and methods

A total of 27 water samples [14 in the piedmont of the Qinling Mountains (QL) and 13 from the Lantian-Bahe Group (LB)] were collected. The sampling locations are shown in Fig. 1. Sampling date, chemical compositions, physicochemical characteristics and hydrochemical types of all water samples are summarized in Table 1. Physicochemical parameters, such as water temperature, pH and total dissolved solids (TDS), were tested immediately in the field using portable meters. Each sample was split between two polyethylene bottles. One bottle was designated for the cation analysis and it was treated with pure nitric acid until a pH below 2 was obtained. The second bottle was for the anion analysis. All water samples were stored at 4 °C. Concentrations of major cations (Na^+ , K^+ , Ca^{2+} and Mg^{2+}) and SiO_2 were analyzed using an AA-100 atomic absorption spectrometer (AAS) with 2–5% accuracy. Anion concentrations were determined using ion chromatography with instrumental error < 5%. Eight samples (Q6, Q7, Q9, Q13, L6, L11, L12 and L13) were collected for measuring isotopic contents of δD and $\delta^{18}\text{O}$ (Table 1), which were analyzed at the Institute of Geology and Geophysics, Chinese Academy of Sciences. δD and $\delta^{18}\text{O}$ values were reported in δ (‰) units with measurement accuracies of 1‰ and 0.2‰, respectively. Factor analysis of the physicochemical data was determined by PCA using IBM SPSS Statistics 20 software.

Results and discussion

Hydrogeochemistry

Water samples were weakly alkaline with a pH range of 7.2–8.3 except for the Q1, Q3 and Q5 samples (Table 1). The average temperature, TDS and SiO_2 concentration measured in QL samples were 41.8 °C, 376.8 mg/L and 38.9 mg/L, respectively. The average temperature, TDS and SiO_2 concentration of LB group were higher: 72.7 °C, 3091.2 mg/L and 45.5 mg/L, respectively. Cationic concentrations of both QL and LB decreased in the order $\text{Na}^+ > \text{Ca}^{2+} > \text{Mg}^{2+} > \text{K}^+$ (Fig. 2). Chemical parameters for LB samples varied more comparing to the QL samples. Anionic concentrations were significantly different between QL and LB. Their concentrations decreased in the order $\text{HCO}_3^- > \text{SO}_4^{2-} > \text{Cl}^-$ for QL and $\text{Cl}^- > \text{SO}_4^{2-} > \text{HCO}_3^-$ for LB.

A Piper diagram serves as a tool for easy classification and comparison of water types (Li et al. 2016a, b).

According to Fig. 3, major cations in QL were sodium and calcium and sodium in LB. Geothermal waters contained mainly bicarbonates and sulfates in QL and chlorides and sulfates in BL. Thus, geothermal water of QL was $\text{HCO}_3\text{--SO}_4\text{--Ca--Na}$, $\text{HCO}_3\text{--SO}_4\text{--Na--Ca}$ and $\text{SO}_4\text{--HCO}_3\text{--Na}$ types. The LB geothermal water was characterized by $\text{SO}_4\text{--Cl--Na}$ and Cl--Na types. The geothermal water of QL has the characteristics of shallow low-temperature geothermal water with the meteoric water recharge in the north piedmont of the Qinling Mountains. Ma et al. (2017) also concluded that the geothermal water in an open and cold geological environment was mixed with some modern meteoric water from the north piedmont of the Qinling Mountains. The Qinling North Piedmont fault, the Yuxia-Tieluzi fault and the Chang'an-Lintong fault provide a favorable channel for the geothermal water in the piedmont of the Qinling Mountains to supply the LB geothermal water. In other words, they provide an effective way for the lateral runoff of QL geothermal water. Besides, water types radically changed from $\text{HCO}_3\text{--Na}$, $\text{SO}_4\text{--Na}$ to Cl--Na in the south of the Guanzhong Basin, indicating that geothermal fluids have a certain degree of hydraulic connection through the major faults. Furthermore, the widespread existence of $\text{SO}_4\text{--Na}$ geothermal water indicates that there is a direct or indirect hydraulic connection between the QL geothermal water and the Cenozoic geothermal water (Zhao 2009).

Principal components analysis (PCA)

Principal components analysis (PCA) is a powerful method for detection of association among variables allowing to reduce the number of dimensions (Zhang et al. 2014). When the accumulative variance was > 0.7 or eigenvalue was ≥ 1 , the covered principal components remained. We systematically analyzed characteristics of QL and LB geothermal waters. 11 variables of the 27 samples revealed some geochemical processes that can lead to the dissolution and precipitation of some minerals. Three factors were extracted with a cumulative variance of 85.99% (Table 2). The variance of the main factor 1 accounted for 54.96%, which was affected by positive loadings of TDS, Na^+ , K^+ , Ca^{2+} , Cl^- , SO_4^{2-} and Mg^{2+} . Correlations coefficients between TDS and Na^+ , K^+ , Ca^{2+} , Cl^- , SO_4^{2-} and Mg^{2+} were relatively high with a significant level test of 0.01 (Table 3). TDS values were virtually determined by these six ions. Factor 2 with positive loadings of T , SiO_2 and pH explained 21.06% of the total variance. Correlations coefficient of T and SiO_2 also passed a significant level test of 0.01. Factor 3 explained 9.97% of total variance and had a positive loading of HCO_3^- .

Table 1 Chemical and isotopic compositions and physicochemical characteristics of geothermal water samples in study area. Q and L represent the QL water samples and LB water samples, respectively

Sampling ID	Well depth (m)	Sampling date	T (°C)	pH	TDS (mg/L)	K ⁺ (mg/L)	Na ⁺ (mg/L)	Ca ²⁺ (mg/L)	Mg ²⁺ (mg/L)	Cl ⁻ (mg/L)	SO ₄ ²⁻ (mg/L)	HCO ₃ ⁻ (mg/L)	SiO ₂ (mg/L)	Water type	Δd (‰)	δ ¹⁸ O (‰)
Q1	N/A	14.03.2007	20	6.8	254.1	0.8	27.4	59.1	6.1	14.2	57.6	177.0	26.6	HCO ₃ ⁻ SO ₄ ⁻	N/A	N/A
Q2	N/A	14.03.2007	29	7.5	217.8	0.8	33.4	49.1	3.6	3.5	16.8	219.7	25.1	HCO ₃ ⁻ Ca-Na	N/A	N/A
Q3	N/A	14.03.2007	20	6.9	266.5	1.4	50.9	42.1	3.4	14.2	75.9	152.5	22.4	HCO ₃ ⁻ SO ₄ ⁻ Na-Ca	N/A	N/A
Q4	N/A	14.03.2007	22	7.3	289.7	0.8	35.2	69.1	6.9	21.3	37.0	238.0	22.5	HCO ₃ ⁻ Ca-Na	N/A	N/A
Q5	N/A	14.03.2007	16	6.4	207.8	0.8	17.2	58.1	3.6	7.1	72.0	97.6	14.9	HCO ₃ ⁻ SO ₄ ⁻	N/A	N/A
Q6	1450.0	12.2005	29	7.2	671.8	7.5	83.9	125.2	33.4	63.8	136.9	442.3	18.9	HCO ₃ ⁻ SO ₄ ⁻ Ca-Na	-70.36	-8.03
Q7	1114.4	12.2005	39.2	8.0	754.0	2.0	230.5	21.1	7.2	63.8	403.5	51.9	30.9	SO ₄ ⁻ Mg	-76.80	-11.53
Q8	350.0	1993	73	8.2	467.2	2.6	146.5	8.0	10.9	21.3	235.1	85.4	80.6	SO ₄ ⁻ Na	N/A	N/A
Q9	650.0	10.07.1998	43	7.5	244.9	2.5	63.0	26.5	3.4	3.5	40.8	195.3	39.2	HCO ₃ ⁻ Na-Ca	-81.83	-11.12
Q10	497.5	31.01.2007	70	7.9	413.3	1.5	136.2	6.0	0.6	30.1	170.5	112.9	46.3	SO ₄ ⁻ HCO ₃ ⁻ Na	N/A	N/A
Q11	514.5	31.01.2007	68	8.1	297.3	1.0	98.5	5.0	0.6	21.3	105.7	115.9	45.7	SO ₄ ⁻ HCO ₃ ⁻ Na	N/A	N/A
Q12	500.0	09.06.1988	40	8.2	163.0	14.2	56.9	15.0	5.2	11.0	50.4	13.9	28.7	SO ₄ ⁻ Na	N/A	N/A
Q13	460.0	1990	55	8.1	567.3	1.7	175.0	11.0	7.2	19.5	319.4	67.1	66.0	SO ₄ ⁻ Ca	-72.85	-10.83
Q14	581.0	21.06.2003	61	8.2	460.1	5.5	160.0	8.0	0.0	34.1	184.9	111.1	76.4	SO ₄ ⁻ HCO ₃ ⁻ Na	N/A	N/A
L1	2010.0	29.01.2007	72	7.8	1974.9	5.1	660.1	25.1	0.6	340.3	830.9	213.6	48.9	SO ₄ ⁻ Na	N/A	N/A
L2	1764.4	29.03.2007	68	7.9	4408.5	9.0	1318.4	97.2	57.1	482.1	2317.0	241.0	30.0	SO ₄ ⁻ Na	N/A	N/A
L3	2503.5	28.03.2007	80.5	7.9	1507.1	5.2	528.9	19.0	0.0	304.9	549.9	183.0	36.5	SO ₄ ⁻ Na	N/A	N/A

Table 1 (continued)

Sampling ID	Well depth (m)	Sampling date	T (°C)	pH	TDS (mg/L)	K ⁺ (mg/L)	Na ⁺ (mg/L)	Ca ²⁺ (mg/L)	Mg ²⁺ (mg/L)	Cl ⁻ (mg/L)	SO ₄ ²⁻ (mg/L)	HCO ₃ ⁻ (mg/L)	SiO ₂ (mg/L)	Water type	Δd (‰)	δ ¹⁸ O (‰)
L4	2370.0	20.03.2007	85	7.9	1322.2	1.5	491.8	6.0	0.0	203.8	333.8	549.2	59.6	HCO ₃ ⁻ SO ₄ ⁻ Cl-Na	N/A	N/A
L5	N/A	16.01.2007	50	7.4	16,023.9	58.3	5498.5	465.9	49.8	6691.2	3182.0	152.5	39.3	Cl-SO ₄ ⁻ Na	N/A	N/A
L6	2128.0	19.09.2002	80	7.5	1869.5	10.0	705.0	8.4	4.8	246.4	429.9	916.5	66.4	HCO ₃ ⁻ SO ₄ ⁻ Cl-Na	-73.49	-6.95
L7	2400.0	25.01.2007	85	7.8	798.6	3.7	283.8	5.0	0.6	198.5	182.5	216.6	46.6	Cl-SO ₄ ⁻ HCO ₃ ⁻ Na	N/A	N/A
L8	2228.0	19.03.2007	81	8.0	889.6	3.8	327.6	6.0	0.6	218.0	199.3	244.1	52.6	Cl-SO ₄ ⁻ HCO ₃ ⁻ Na	N/A	N/A
L9	N/A	28.03.2007	68	8.1	823.2	3.2	284.4	7.6	0.2	102.0	331.4	167.8	33.1	SO ₄ -Cl- HCO ₃ ⁻ Na	N/A	N/A
L10	1708.6	16.01.2007	50	7.8	2200.0	5.5	809.0	22.0	1.2	216.2	658.0	964.1	24.4	HCO ₃ ⁻ SO ₄ -Na	N/A	N/A
L11	3112.0	26.10.2002	84	8.3	695.2	3.5	254.0	16.4	1.0	202.1	175.8	59.8	58.0	Cl-SO ₄ ⁻ Na	-69.74	-8.88
L12	1550.0	1995	50	8.1	844.3	1.7	293.5	7.0	7.2	187.9	290.6	112.9	26.6	SO ₄ -Cl- Na	-76.17	-11.03
L13	2451.0	12.2005	92	7.3	6829.1	4.7	2618.0	61.0	15.6	3456.4	473.1	400.5	69.9	Cl-Na	-56.38	-2.70

N/A not analyzed

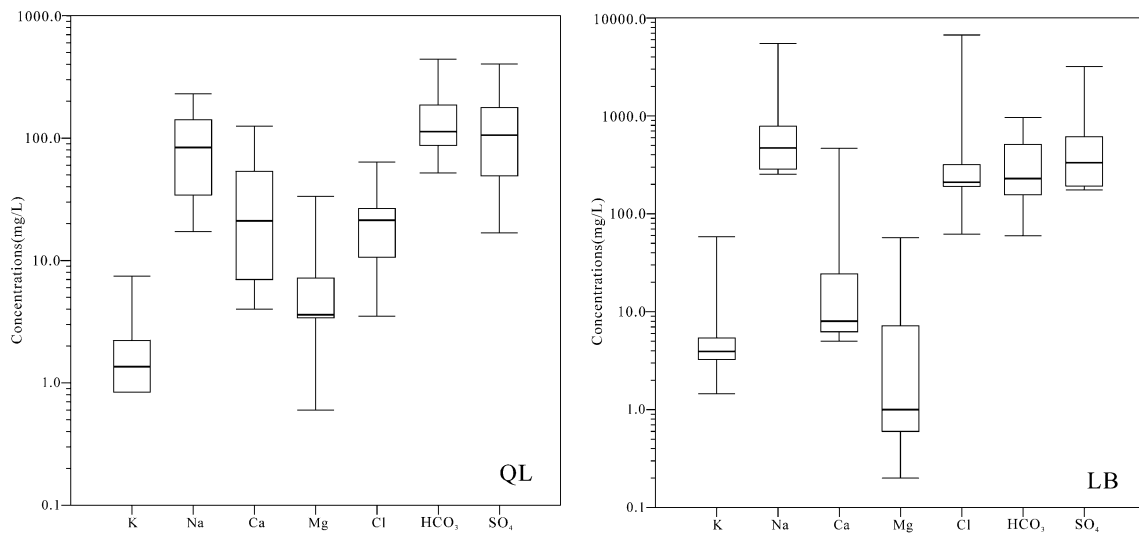


Fig. 2 Box-and-whisker plot of major constituents QL and LB geothermal samples

Fig. 3 Piper diagram of geothermal water samples

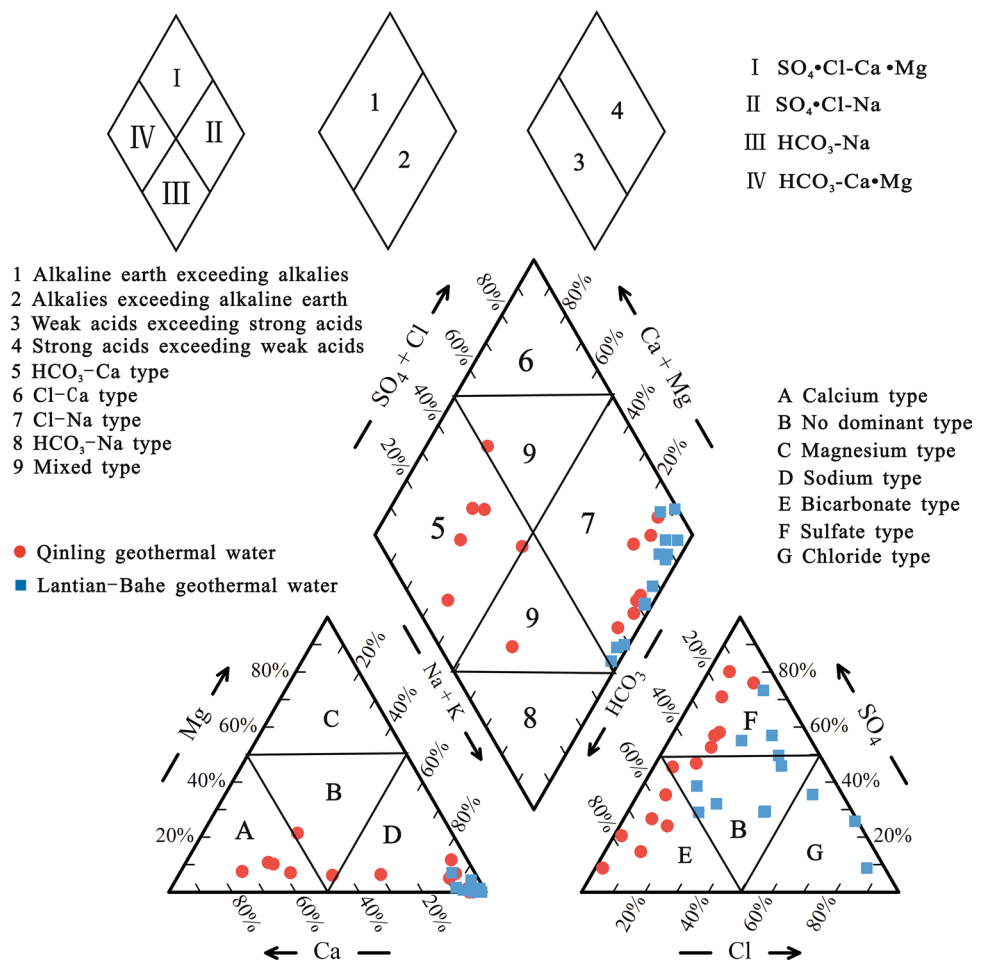


Table 2 Loading of variables on three principal components of geothermal water samples

Variables	Factors		
	1	2	3
T	0.05	0.93	0.11
K ⁺	0.95	0.03	0.01
Na ⁺	0.97	0.14	0.10
Ca ²⁺	0.94	-0.24	-0.11
Mg ²⁺	0.78	-0.15	-0.14
Cl ⁻	0.94	0.11	0.03
SO ₄ ²⁻	0.91	0.08	-0.07
HCO ₃ ⁻	0.03	0.00	0.96
pH	-0.19	0.76	-0.32
TDS	0.98	0.11	0.07
SiO ₂	-0.01	0.86	0.09
Eigen value	6.05	2.32	1.10
Variance (%)	54.96	21.06	9.97
Cumulative (%)	54.96	76.02	85.99

Geochemical genesis of factor 1

In Fig. 4a, all the water samples are scattered below the halite dissolution line suggesting that the sources of Na⁺ were plagioclase weathering and dissolution of halite (Hanor 1994). Values of Na⁺ and Cl⁻ for QL were lower than those for LB, indicating that the weathering and dissolution of the QL geothermal water were weaker. In Fig. 4b, all LB water samples and some QL samples were above the gypsum dissolution line, which was attributed to the oxidation of sulfides in a relatively open hydrogeological environment. Other QL water samples were below the gypsum dissolution line with a higher concentration of Ca²⁺, illustrating that the sources of Ca²⁺ could be calcite, dolomite or silicate and that QL geothermal water was in a hydraulic connection with shallow groundwater (Russak and Sivan 2010). Cation exchange and adsorption were the major processes

in the groundwater with characteristics that Ca²⁺ and Mg²⁺ decreased and Na⁺ and K⁺ increased in the direction of groundwater flow (Jalali 2005). The ion exchange in LB was greater than that in QL which can be seen in Fig. 4c, providing evidence that water–rock interactions were less active in QL. Besides, geothermal fluids flow from the Qinling Mountains piedmont to the central Guanzhong basin. Concentrations of earth metals (Ca²⁺ + Mg²⁺) and HCO₃⁻ exceeded those of alkaline metals (Na⁺ + K⁺) and SO₄²⁻ + Cl⁻, respectively, indicating modern infiltration water origin of the geothermal water, otherwise geothermal water was characterized as a deep underground fluid system (Chadha 1999). In Fig. 4d, it can be indicated that QL geothermal water was recharged with modern infiltration water by fracture structures which provided flow channels for atmospheric precipitation. Compared with the QL, the LB geothermal water was stored in a deeper geothermal system, which was especially evident for the L13 and L5 sampling sites.

The diagram of Ca_{excess}–Na_{deficit}, in which a perfect linear correlation is featured with an approximate slope of 1, is called basinal fluid line (BFL). It reflects the components of fluid and its formation (Davisson et al. 1994; Heijlen et al. 2000; Lee Davisson and Criss 1996). The calculation formula can be described as (1) and (2):

$$Ca_{\text{excess}} = [Ca_{\text{meas}} - (Ca/Cl)_{\text{sw}} \times Cl_{\text{meas}}] \times 2/40.08 \quad (1)$$

$$Na_{\text{deficit}} = [(Na/Cl)_{\text{sw}} \times Cl_{\text{meas}} - Na_{\text{meas}}]/22.99 \quad (2)$$

where Ca_{excess} is Ca²⁺ concentration relative to seawater enrichment (in meq/L), Na_{deficit} is Na⁺ concentration relative to seawater deficit (in meq/L), subscripts of ‘meas’ and ‘sw’ mean concentration of ions in current seawater and samples (in mg/L), respectively. According to Fig. 5, Ca²⁺ of QL was in slight excess and Na⁺ of LB was in slight deficit in the region A, meaning that QL geothermal water was of modern dissolved origin with relatively weak water–rock interactions, while LB geothermal water had a residual sedimentary origin. Na⁺ excess in L13 and L5 samples in the region B

Table 3 Correlation coefficients of the physicochemical parameters

Catalog	T	K ⁺	Na ⁺	Ca ²⁺	Mg ²⁺	Cl ⁻	SO ₄ ²⁻	HCO ₃ ⁻	pH	TDS	SiO ₂
T	1										
K ⁺	0.03	1									
Na ⁺	0.19	0.91	1								
Ca ²⁺	-0.21	0.93	0.86	1							
Mg ²⁺	-0.07	0.65	0.65	0.74	1						
Cl ⁻	0.14	0.89	0.98	0.86	0.58	1					
SO ₄ ²⁻	0.14	0.85	0.85	0.80	0.82	0.75	1				
HCO ₃ ⁻	0.09	0.04	0.09	-0.08	-0.04	-0.01	0.02	1			
pH	0.61	-0.11	-0.13	-0.32	-0.19	-0.17	-0.02	-0.18	1		
TDS	0.16	0.92	0.99	0.88	0.69	0.97	0.87	0.07	-0.14	1	
SiO ₂	0.74	0.02	0.12	-0.19	-0.16	0.12	-0.02	0.01	0.45	0.08	1

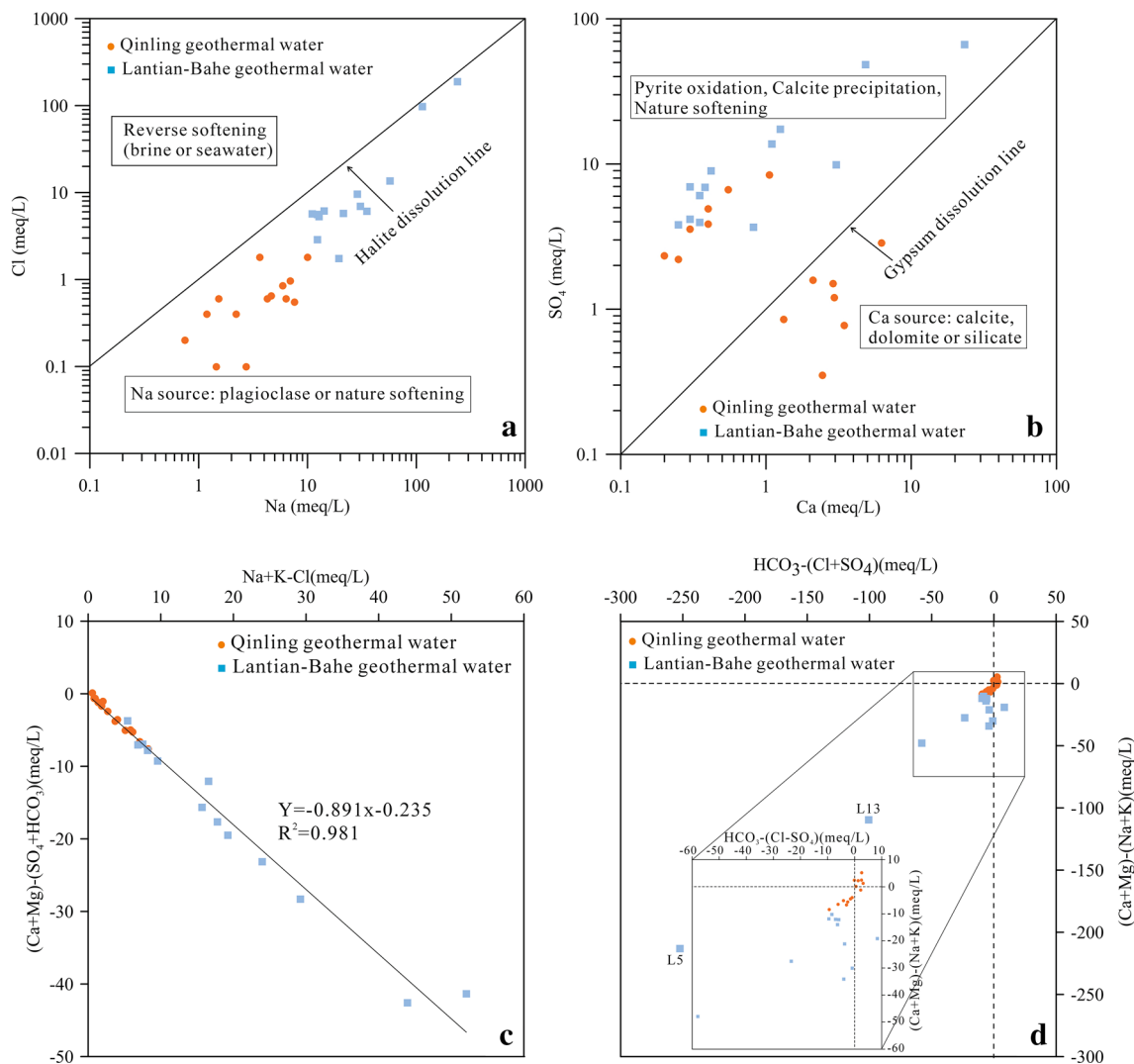


Fig. 4 The scatter diagrams of (a) Cl^- vs. Na^+ , (b) SO_4^{2-} vs. Ca^{2+} , (c) $\text{Na} + \text{K} - \text{Cl}$ vs. $\text{Ca} + \text{Mg} - \text{SO}_4 - \text{HCO}_3$, (d) $\text{HCO}_3 - (\text{Cl} + \text{SO}_4)$ vs. $\text{Ca} + \text{Mg} - \text{K} - \text{Na}$ in all water samples

was due to the bigger depth and a more closed geochemical environment.

Geochemical genesis of factors 2 and 3

In Fig. 6a, SiO_2 concentration positively correlated with temperature passing a significant level test of 0.01. The silica in natural waters was barely affected by other ions and complexes, which was considered as a good indicator for the temperature of thermal reservoir. Figure 6b showed a relationship between $(\text{Ca}^{2+} + \text{Mg}^{2+})$ and HCO_3^- . The 1:1 line was attributed to the dissolution of calcite or dolomite, which was dissolved as HCO_3^- and Ca^{2+} with a 1:1 ratio or as $(\text{Ca}^{2+} + \text{Mg}^{2+})$ and HCO_3^- with a 1:1 ratio as well (Zhang et al. 2016). The most likely sources of $(\text{Ca}^{2+} + \text{Mg}^{2+})$ and HCO_3^- in QL samples, distributed

along the 1:1 line, were calcite and dolomite widely present in the Quaternary strata. LB samples scattered below the 1:1 line, which was related to the strong cation exchange and adsorption.

Ion ratios and hydrochemical coefficients

Values of the hydrochemical parameters were calculated to determine water origin and to detect hydrochemical processes in water (Abdel Moneim et al. 2015; El-Aassy et al. 2015; Li et al. 2018d). Ion ratios and hydrochemical coefficients, expressed as $r\text{Na}^+/\text{rCl}^-$, $r\text{SO}_4^{2-} \times 100/\text{rCl}^-$, $r\text{Ca}^{2+}/r\text{Mg}^{2+}$ and $r\text{Mg}^{2+}/r\text{Cl}^-$, were obtained for geothermal waters of QL and LB. A summary of the calculation of these parameters is presented in Table 4.

Fig. 5 The scatter diagram of $Ca_{\text{excess}} - Na_{\text{deficit}}$ of geothermal water

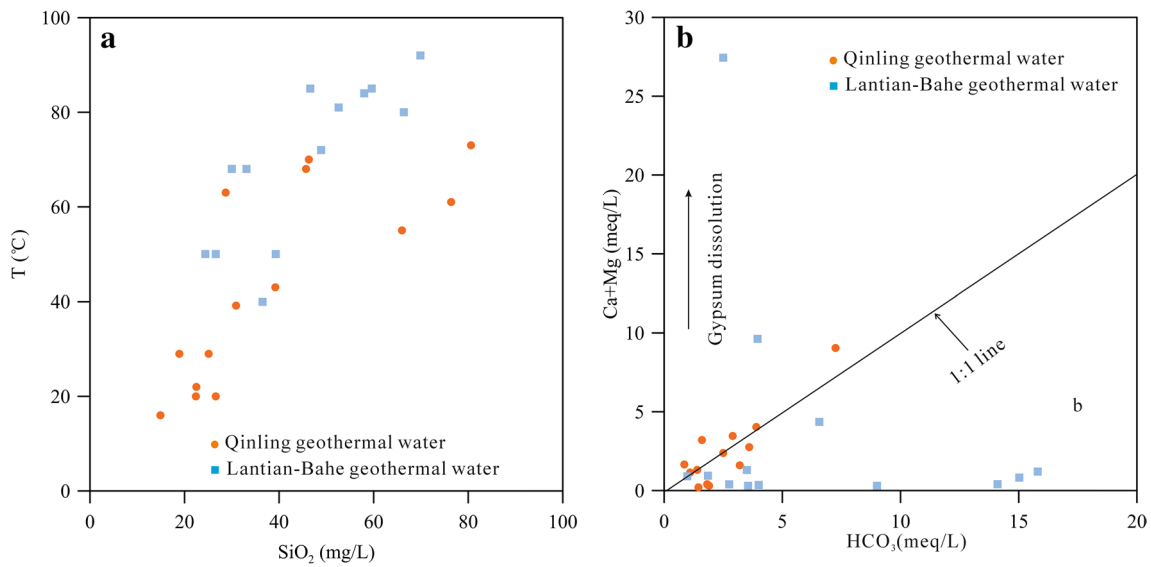
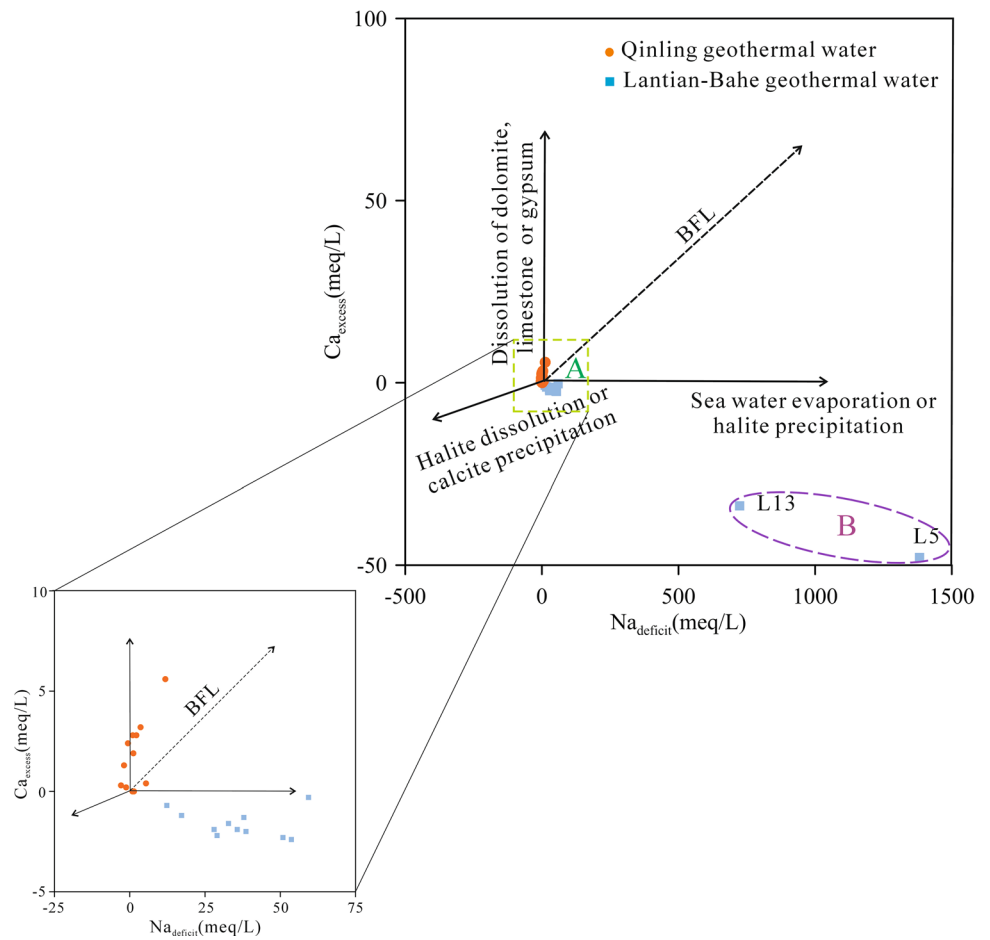


Fig. 6 The scatter diagrams of (a) T vs. SiO_2 , HCO_3^- vs. Ca + Mg in geothermal water

Table 4 The range and mean of hydrochemical parameters in geothermal water

District	Parameters	$r\text{Na}^+/\text{rCl}^-$	$\text{rSO}_4^{2-} \times 100/\text{rCl}^-$	$\text{rCa}^{2+}/\text{rMg}^{2+}$	$\text{rMg}^{2+}/\text{rCl}^-$
QL ($n = 14$)	Range	2.03–27.78	300.00–1211.40	0.44–9.68	0.06–3.04
	Mean	8.42	499.42	4.85	1.25
BL ($n = 13$)	Range	1.17–11.14	10.12–355.45	0.58–25.10	0.01–0.35
	Mean	3.68	141.35	8.11	0.05

Metamorphic coefficient (MC) $r\text{Na}^+/\text{rCl}^-$

$r\text{Na}^+/\text{rCl}^-$ ratio is an essential indicator for degree of stratification and metamorphism of the groundwater and sealing of hydrogeochemical environment of the reservoir (Zhang 2016). The smaller the MC is, the better the reservoir environment sealing property will be, reflecting the relatively reductive water environment (Zhang 2016). MC is also used in detecting the groundwater origin (marine or meteoric) (Abdel Moneim et al. 2015). All the samples had $\text{MC} > 1$ suggesting meteoric origin of the geothermal water. The average MC value of QL equal to 8.42 was larger than that of LB (3.68) indicating a stronger influence of meteoric water on geothermal water of QL as well as that the reservoir environment was more open, because the fracture structures, mainly including the Qinling North Piedmont fault, the Yuxia-Tieluzi fault, and the Chang'an-Lintong fault, provided flow channels for atmospheric precipitation (Fig. 1). The MC increased from the center to the border of the basin, namely from LB to QL. However, excess of chloride and sodium in LB was attributed to the leaching and ionic exchange in the direction of the centripetal flow in the basin.

Desulfurization coefficient (DC) $\text{rSO}_4^{2-} \times 100/\text{rCl}^-$

Desulfurization coefficient ($100 \times \text{rSO}_4^{2-}/\text{rCl}^-$) is a useful indicator to measure the redox environment in deep groundwater and to evaluate the strength of desulfurization and the degree of closure of the groundwater environment (Zhang 2016). DC of groundwater was greater than DC of normal seawater (equal to 10.26) indicating an open geological environment (Zhang 2016). Only DC of the sample L13 (10.12) was less than 10.26, which was due to a closed reservoir environment. It is generally accepted that the smaller the DC is, the better the closure of the formation will be. The average value of QL (499.42) was far greater than that of LB (141.35) suggesting that the geological environment of QL was open.

$\text{rCa}^{2+}/\text{rMg}^{2+}$ parameter

$\text{rCa}^{2+}/\text{rMg}^{2+}$ parameter positively correlated with the storage time of geothermal water, and its high values are mainly attributed to the dissolution, ion exchange or fresh water

recharging (El-Aassy et al. 2015; Zhang 2016). The average values of $\text{rCa}^{2+}/\text{rMg}^{2+}$ of QL and LB were 4.85 and 8.11, respectively, indicating that the geothermal water residence time of QL was shorter and its circulation was faster.

$\text{rMg}^{2+}/\text{rCl}^-$ parameter

$\text{rMg}^{2+}/\text{rCl}^-$ parameter is of special importance and is used in detecting water origin and mixing processes. $\text{rMg}^{2+}/\text{rCl}^-$ values of fresh water are slightly above 0.5, but the groundwater has values of $\text{rMg}^{2+}/\text{rCl}^-$ below 0.5 (Custudio and Bruggeman 1987). The $\text{rMg}^{2+}/\text{rCl}^-$ of QL geothermal water ranged from 0.06 to 3.04 with an average value of 1.25. 75% of the QL samples had $\text{rMg}^{2+}/\text{rCl}^-$ parameter higher above 0.5, while the same parameter for the remaining 25% of samples was below 0.5 indicating that geothermal water had the origin of atmospheric precipitation and was highly mixed with shallow cold waters. Thus, the temperature of the QL geothermal water was relatively low. However, $\text{rMg}^{2+}/\text{rCl}^-$ (ranging from 0.01 to 0.35) of all LB water samples was less than 0.5 indicating deep groundwater characteristics.

Characteristics and distribution of stable isotopes

Stable isotopes of hydrogen and oxygen are important tracers used to study the origin and circulation of water bodies and have been applied in many studies (Qian et al. 2013, 2014; Li et al. 2016c). Particularly, the origin and circulation of the geothermal water system can be identified by the evaluation of δD and $\delta^{18}\text{O}$ (Sanliyuksel and Baba 2011). The degree of oxygen shift and deuterium surplus is dependent on the reservoir temperature, residence time and water–rock interactions (Sanliyuksel and Baba 2011; Wang et al. 2013). The QL geothermal water had the mean compositions of δD and $\delta^{18}\text{O}$: -75.46‰ and -10.38‰ . As for LB geothermal water, the compositions of δD and $\delta^{18}\text{O}$ were higher with average values of -68.95‰ and -7.39‰ , which indicated the LB geothermal reservoir had high temperatures and strong water–rock interactions. The relationship between δD and $\delta^{18}\text{O}$ for geothermal water samples is shown in Fig. 7. Data points corresponding to the water samples (Q7, Q9, Q13, L12) of region A spread along the global meteoric water line (GMWL) and local meteoric water line (LMWL), indicating that the geothermal water was controlled by

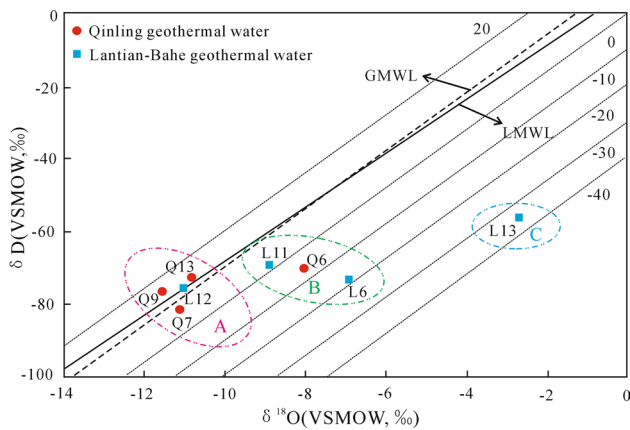


Fig. 7 The δD – $\delta^{18}O$ diagram of geothermal water in the study area. GMWL is the global meteoric water line, $\delta D = 8\delta^{18}O + 10$ (Craig 1961). LMWL is the local meteoric water line, $\delta D = 7.5\delta^{18}O + 6.1$, based on the data from the GNIP network at Xi’an station

meteoric water, namely, it had the recharge origin of precipitation. In region B, water samples (Q6, L6, L11) with a slight oxygen shift were due to a larger degree of water–rock interactions in half-closed thermal environment with a big depth. The source types of water samples in the two regions of A and B were not completely independent, which indicated that the QL and LB geothermal water had the hydraulic connection through the major faults. This also provided strong evidence for the recharge of the LB geothermal water by geothermal water in the piedmont of the Qinling Mountains. For region C, the L13 sample was far away from the GMWL and LMWL with a significant $\delta^{18}O$ shift, suggesting that the geothermal water system was closed with long

residence time. This type of water was characterized by the origin of the residual sedimentary water and ancient lixiviation water (Ma et al. 2017). Furthermore, combined with the sedimentary environment of the Guanzhong Basin, the ranges of $\delta^{18}O$ and δD values of sedimentary water in the Guanzhong Basin are $-100\text{‰} \sim -45\text{‰}$ and $-4.5\text{‰} \sim 3\text{‰}$, respectively (He 2015). It can be inferred that the L13 sample ($\delta D = -56.38\text{‰}$, $\delta^{18}O = -2.70\text{‰}$) had the characteristics of sedimentary water.

The mixing process of geothermal water can be understood by correlating chemical features with isotopic features (Avsar et al. 2016). The diagrams of Cl^- vs. δD and Cl^- vs. $\delta^{18}O$ are shown in Fig. 8. The geothermal water and rainwater samples in the piedmont of the Qinling Mountains basically were located in the same area, with low content of Cl^- , δD and $\delta^{18}O$, which also proved that the QL geothermal water had the recharge of atmospheric precipitation. The content of Cl^- , δD and $\delta^{18}O$ in the LB geothermal water samples (except L13) was slightly high, indicating that it was mainly supplied by the piedmont of the Qinling Mountains, and the proportion of mixed meteoric precipitation was relatively reduced. However, the Cl^- content of L13 sample was exceptionally high with the enrichment of deuterium and oxygen. It indicated the geothermal water was formed in a closed environment and had little connection with modern meteoric precipitation, which conformed to the characteristics of ancient infiltration water or sedimentary water.

The relationship of $\lg Cl^- - \delta^{18}O$ can describe clearly the reservoir environment and the genetic classification of geothermal water (see Fig. 9) (Su 2008; Xu 2014). The I–II line represents the cycling-type geothermal water line, which shows that the mixing proportion of modern infiltration

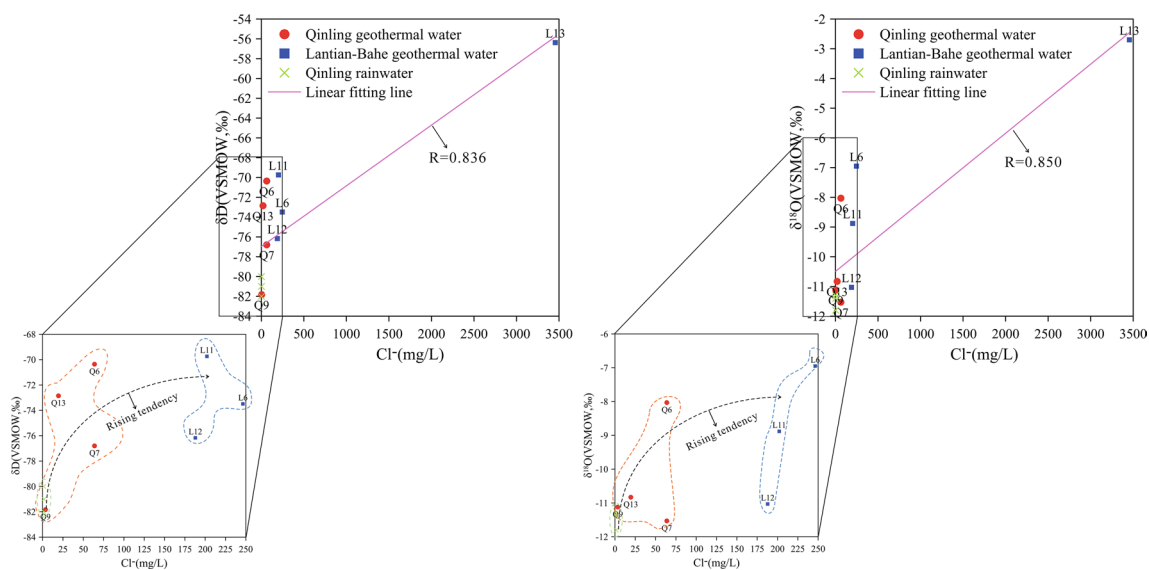


Fig. 8 The diagrams of Cl^- vs. δD and Cl^- vs. $\delta^{18}O$. Qinling rainwater samples are from He (2015)

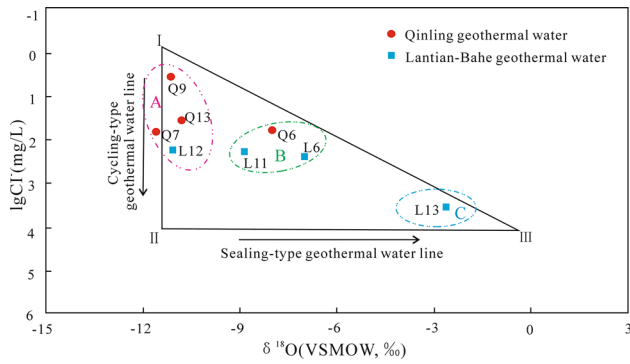


Fig. 9 The $\lg\text{Cl}^- - \delta^{18}\text{O}$ diagram of geothermal water in the study area. The points of I, II and III indicate modern infiltration water, ancient infiltration water and sealing-type water Refer from: Xu (2014)

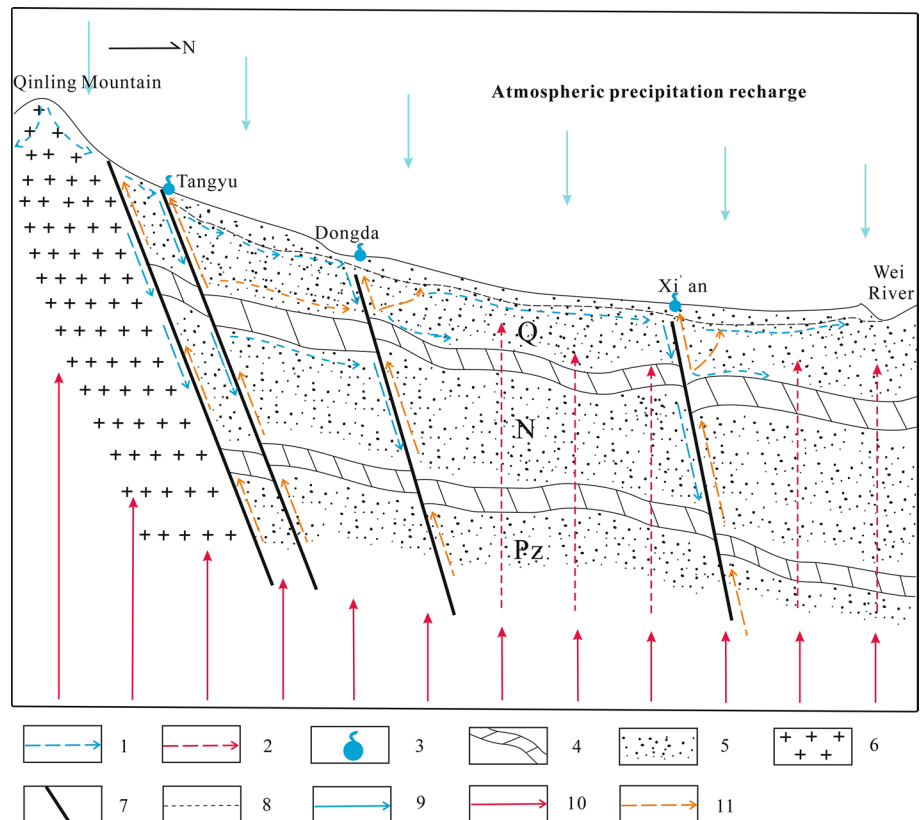
water gradually decreases from I point to II point; the II–III line is the sealing-type geothermal water line, explaining that the geological environment of geothermal water is more closed, and the connection between geothermal water and modern leachate water is weakened from II point to III point; the water sample points inside the triangle represent the mixed water of three types (I, II and III) (Su 2008; Xu 2014). The QL water samples, located near the region A, revealed that the dominant origin of the QL geothermal water was

modern infiltration water, followed by a small amount of ancient lixiviation water. Its geothermal reservoir was in an open geological environment. The LB water samples were mainly distributed in the region B, which is in the interior of the triangle. It indicated the LB geothermal water which was formed in a semi-closed geological environment was mixed water of ancient lixiviation water, modern infiltration water and sealing-type water, and the dominated origin was ancient lixiviation water. As for region C (L13 sample), the geological environment was closed and the dominant origin of geothermal water was sealing-type water with the characteristics of sedimentary water.

Geothermal formation pattern

Figure 10 shows a brief pattern of geothermal formation between the piedmont of the Qinling Mountains and the central Guanzhong Basin. The geothermal formation model of QL belongs to the vertical convection pattern. Deep thermal energy is carried by the fluid due to the openness of the fault and migrates along the fault zone to the surface, and shallow cold water is mixed (Mu et al. 2016). From Tangyu to Dongda, the major pattern is the horizontal convection pattern. It is characterized by the fact that the geothermal fluid flows in a horizontal manner due to the obstruction of the upper passage during the vertical convection along the

Fig. 10 Brief pattern of geothermal formation between the piedmont of Qinling Mountains and central Guanzhong Basin. 1: cold water flow direction; 2: thermal conduction direction; 3: hot spring; 4: aquiclude; 5: aquifer; 6: bedrock; 7: fault; 8: water table; 9: atmospheric precipitation; 10: geothermal source; 11: geothermal water flow direction Refer from: Mu et al. (2016)



fault zone (Mu et al. 2016), thus, the piedmont region of the Qinling Mountains can be a replenishment of the geothermal water in central Guanzhong. A vertical conduction model with a deep heat source that is diffused to the surface by conduction is dominant between Dongda and Wei River. Thus, it can be seen that faults can provide the effective channels for the flow of geothermal water and cold water. The overlying strata of the thermal reservoir are thick with a good waterproof effect, so the heat conduction (the mode of transport without material participation) can transfer heat vertically. In brief, geothermal formation patterns are followed by vertical convection, horizontal convection and vertical conduction from the piedmont of the Qinling Mountains to the central Guanzhong Basin.

Geothermometer application

Figure 11 indicates that QL geothermal water was immature water and LB geothermal water was immature water or partially equilibrated water. All water samples concentrated in Mg corner, providing the evidence that the geothermal water was blended with a high extent of cold water during the process of rising from heat source to the surface (Lajwe 2014). Silica geothermometers can be utilized to predict the temperature of low-temperature geothermal systems (Fournier 1977). Cationic geothermometers, mainly including Na–K (Giggenbach 1988), K–Mg (Giggenbach 1988), Na–K–Ca (Fournier and Truesdell 1973) and Na–K–Ca–Mg corrected (Fournier and Potter 1978), could not be used to calculate a reasonable temperature value, because geothermal water samples were plotted outside the full equilibrium area. Furthermore, no samples within the mature water area region on the graph are found in Fig. 12, indicating that cationic geothermometers were also inappropriate (Giggenbach 1991).

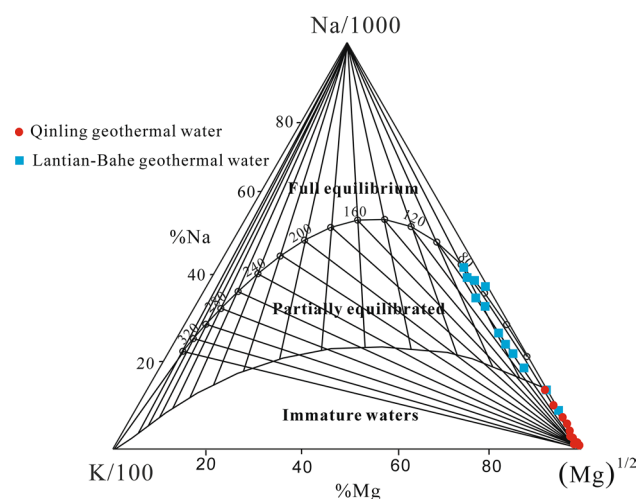


Fig. 11 Ternary diagram of Na–K–Mg concentrations in geothermal waters

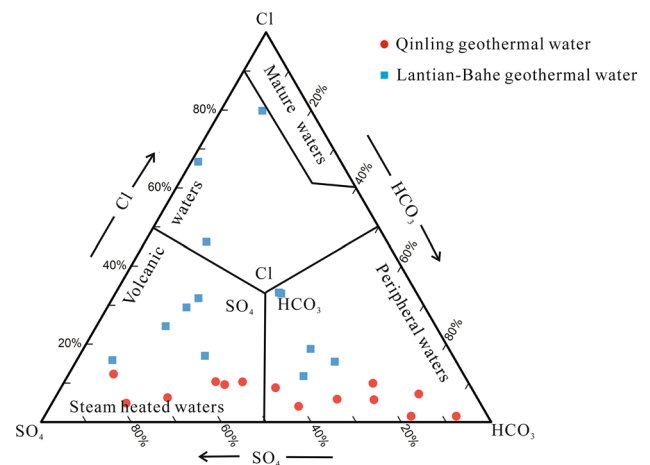


Fig. 12 Ternary diagram of Cl–SO₄–HCO₃ concentrations in geothermal waters

Table 5 The results of silica geothermometers, units in °C

Sample label	Observed	Quartz ^a	Quartz ^b	Chalcedony ^c	α Cristobalite ^d
Q1	20	74.5	78.7	42.9	24.9
Q2	29	72.2	76.7	40.5	22.7
Q3	20	67.8	72.8	35.9	18.4
Q4	22	67.9	72.9	36.0	18.6
Q5	16	52.7	59.4	20.3	4.1
Q6	29	61.3	67.1	29.2	12.3
Q7	39.2	80.6	84.1	49.3	30.8
Q8	73	125.5	122.8	97.6	74.8
Q9	43	90.8	93.0	60.1	40.7
Q10	70	98.3	99.5	68.1	47.9
Q11	68	97.7	99.0	67.4	47.4
Q12	40	77.6	81.5	46.1	27.9
Q13	55	115.2	114.1	86.4	64.6
Q14	61	122.7	120.4	94.5	72.0
L1	72	100.8	101.7	70.8	50.4
L2	68	79.4	83.1	48.1	29.6
L3	80.5	87.7	90.3	56.8	37.6
L4	85	110.2	109.8	80.9	59.7
L5	80	115.5	114.3	86.7	64.9
L6	85	98.6	99.7	68.4	48.2
L7	81	104.2	104.6	74.4	53.8
L8	68	83.5	86.6	52.4	33.6
L9	50	71.1	75.7	39.3	21.6
L10	84	108.9	108.6	79.5	58.4
L11	50	74.5	78.7	42.9	24.9
L12	92	118.1	116.6	89.5	67.5

^aFournier and Potter (1982) no steam loss

^bFournier (1977) maximum steam loss 100 °C

^{c, d}Morey et al. (1962)

By comparing results of four silica geothermometers with observed data (shown in Table 5), the reservoir temperature of QL was estimated more reliably by the chalcedony geothermometer and it ranged from 20.3 to 97.6 °C. Additionally, considering that the water temperature was below 100 °C and not taking steam loss of SiO₂ into consideration, the reservoir temperature in LB calculated by Quartz^a was in the 75.7–116.6 °C range. Our calculated results showed that the temperature range was large, because geothermal water could be mixed with different ratios of subsurface cold water.

Conclusions

We analyzed principal components and performed a comparative analysis of isotopic and hydrogeochemical characteristics of geothermal water. Based on this analysis, we demonstrated a clear distinction between QL and LB geothermal waters. From the piedmont of the Qinling Mountains to the Lantian-Bahe Group of the central Guanzhong Basin, water types change from HCO₃-Na, SO₄-Na to Cl-Na, indicating that geothermal fluids of QL and LB have a hydraulic connection. The geothermal fluids of QL could be a recharge source of LB geothermal fluids.

According to the relationships between the three principal factors based on PCA and representative hydrochemical parameters (such as rNa⁺/rCl⁻, rSO₄²⁻×100/rCl⁻, rCa²⁺/rMg²⁺ and rMg²⁺/rCl⁻), the residence time of QL geothermal water is shorter than that of LB. The circulation of QL geothermal water is faster, and its water–rock interactions are weaker in an open and oxidized geological environment. The major origin of QL geothermal water is modern infiltration water, since geological structures provide water with channels for atmospheric precipitation. The second water origin in QL is ancient lexiviation water. LB geothermal water has ancient lexiviation water and modern infiltration water origin. It might also originate from the residual sedimentary water. Isotopic evidence of δD–δ¹⁸O, Cl⁻–δD, Cl⁻–δ¹⁸O and lgCl⁻–δ¹⁸O also demonstrates that geological environment of LB is semi-closed or closed. The reservoir temperature of QL estimated by the chalcedony geothermometer ranges from 20.3 to 97.6 °C. The reservoir temperature in LB calculated by Quartz^a is 75.7–116.6 °C. The geothermal formation model of QL is mainly the vertical convection, followed by horizontal convection, and the formation of LB geothermal water is dominated by vertical heat conduction.

Hydrogeochemical methods and principal components analysis of QL and LB geothermal water provide confidence in identifying the extent of water–rock interactions and mixing processes with the shallow cold water, water types of origin and evaluation of geotemperatures. However,

for interpretation of the origin of geothermal water, determination of groundwater age based on the isotope analysis is recommended. This study hopes to provide guidance for the survey and evaluation of geothermal resources in the Qinling Mountains piedmont, the Lantian-Bahe Group in the Guanzhong Basin and other similar areas worldwide.

Acknowledgements This study was financially supported by the National Natural Science Foundation of China (Grant No. 41572236), which is gratefully acknowledged. Anonymous reviewers and the Editor are sincerely thanked for their constructive comments on the earlier versions of this paper.

References

- Abdel Moneim AA, Seleem EM, Zeid SA, Abdel Samie SG, Zaki S, Abu El-Fotoh A (2015) Hydrogeochemical characteristics and age dating of groundwater in the Quaternary and Nubian aquifer systems in Wadi Qena, Eastern Desert, Egypt. *Sustain Water Resour Manag* 1(3):213–232. <https://doi.org/10.1007/s40899-015-0018-3>
- Avsar O, Kurtulus B, Gursu S, Kuscü GG, Kacaroglu F (2016) Geochemical and isotopic characteristics of structurally controlled geothermal and mineral waters of Mugla (SW Turkey). *Geothermics* 64:466–481. <https://doi.org/10.1016/j.geothermics.2016.06.020>
- Baumann T, Bartels J, Lafogler M, Wenderoth F (2017) Assessment of heat mining and hydrogeochemical reactions with data from a former geothermal injection well in the Malm Aquifer, Bavarian Molasse Basin, Germany. *Geothermics* 66:50–60. <https://doi.org/10.1016/j.geothermics.2016.11.008>
- Blasco M, Auque LF, Gimeno MJ, Acero P, Asta MP (2017) Geochemistry, geothermometry and influence of the concentration of mobile elements in the chemical characteristics of carbonate-evaporitic thermal systems. The case of the Tiermas geothermal system (Spain). *Chem Geol* 466:696–709. <https://doi.org/10.1016/j.chemgeo.2017.07.013>
- Chadha DK (1999) A proposed new diagram for geochemical classification of natural waters and interpretation of chemical data. *Hydrogeol J* 7(5):431–439. <https://doi.org/10.1007/s100400050>
- Craig H (1961) Isotopic Variations in Meteoric Waters. *Science* 133(3465):1702–1703. <https://doi.org/10.1126/science.133.3465.1702>
- Custodio E, Bruggeman GA, Cotecchia V (1987) Groundwater problems in coastal areas. *Studies and reports in hydrology*, vol. 35. UNESCO, Paris. <http://www.fao.org/library/library-home/en/>
- Dassi L (2011) Investigation by multivariate analysis of groundwater composition in a multilayer aquifer system from North Africa: a multi-tracer approach. *Appl Geochem* 26(8):1386–1398. <https://doi.org/10.1016/j.apgeochem.2011.05.012>
- Davissou ML, Presser TS, Criss RE (1994) Geochemistry of tectonically expelled fluids from the northern Coast ranges, Rumsey Hills, California, USA. *Geochim Cosmochim Acta* 58(7):1687–1699. [https://doi.org/10.1016/0016-7037\(94\)90530-4](https://doi.org/10.1016/0016-7037(94)90530-4)
- Davraz A, Aksever F, Afsin M (2017) Assessment of stream water chemistry and impact of geothermal fluid in the up-Buyuk Menderes Basin, Turkey. *Environ Sci Pollut Res* 24(34):26806–26820. <https://doi.org/10.1007/s11356-017-0302-x>
- Duan L, Wang WK, Sun YB, Zhang CC (2016) Iodine in groundwater of the Guanzhong Basin, China: sources and hydrogeochemical controls on its distribution. *Environ Earth Sci*. <https://doi.org/10.1007/s12665-016-5781-4>

- El-Aassy IK, El-Feky M, Issa FA, Ibrahim NM, Desouky O, Khatab M (2015) Characterization of groundwater and uranium isotopic ratios ($^{234}\text{U}/^{238}\text{U}$) in some dug and drilled wells from southwestern Sinai, Egypt. *Eur J Water Qual* 9:19–30
- Etzel TM, Bowman JR, Moore JN, Valley JW, Spicuzza MJ, McCulloch JM (2017) Oxygen isotope systematics in an evolving geothermal system: Coso Hot Springs, California. *J Volcanol Geoth Res* 329:54–68. <https://doi.org/10.1016/j.jvolgeores.2016.11.014>
- Fournier RO (1977) Chemical geothermometers and mixing models for geothermal systems. *Geothermics* 5(1):41–50. [https://doi.org/10.1016/0375-6505\(77\)90007-4](https://doi.org/10.1016/0375-6505(77)90007-4)
- Fournier RO, Potter RWI (1978) Magnesium correction for the Na–K–Ca chemical geothermometer, USGS-OFR-78-986. Geological Survey, Menlo Park
- Fournier RO, Potter RWI (1982) Revised and expanded silica (quartz) geothermometer. *Geotherm Resour Counc Bull* 11:3–12
- Fournier RO, Truesdell AH (1973) An empirical Na–K–Ca geothermometer for natural waters. *Geochim Cosmochim Acta* 37(5):1255–1275. [https://doi.org/10.1016/0016-7037\(73\)90060-4](https://doi.org/10.1016/0016-7037(73)90060-4)
- Giggenbach WF (1988) Geothermal solute equilibria. derivation of Na–K–Mg–Ca geothermometers. *Geochim Cosmochim Acta* 52(12):2749–2765. [https://doi.org/10.1016/0016-7037\(88\)90143-3](https://doi.org/10.1016/0016-7037(88)90143-3)
- Giggenbach WF (1991) Chemical techniques in geothermal exploration. In: D'Amore F (editor) Application of geochemistry in geothermal reservoir development. UNITAR/UNDP publication, Rome, pp 119–144. <https://ci.nii.ac.jp/naid/10008803480/en/>
- Guo QH, Wang YX (2012) Geochemistry of hot springs in the Tengchong hydrothermal areas, Southwestern China. *J Volcanol Geoth Res* 215:61–73. <https://doi.org/10.1016/j.jvolgeores.2011.12.003>
- Hanor JS (1994) Origin of saline fluids in sedimentary basins. *Geol Soc Lond Spec Publ* 78(1):151–174. <https://doi.org/10.1144/gsl.sp.1994.078.01.13>
- He D (2015) Isotopic and hydrogeochemical Evidence of remaining sedimentary water in the deep geothermal reservoir of Guanzhong Basin. MS thesis, Chang'an University, Xi'an, China (in Chinese)
- Heijlen W, Muchez P, Banks D, Nielsen P (2000) Origin and geochemical evolution of synsedimentary, syn- and post-tectonic high-salinity fluids at the Variscan thrust front in Belgium. *J Geochem Explor* 69–70:149–152. [https://doi.org/10.1016/S0375-6742\(00\)00018-2](https://doi.org/10.1016/S0375-6742(00)00018-2)
- Jalali M (2005) Major ion chemistry of groundwaters in the Bahar area, Hamadan, western Iran. *Environ Geol* 47(6):763–772. <https://doi.org/10.1007/s00254-004-1200-3>
- Lajwe G (2014) Comparison, characterization, and interpretation of geothermal fluid geochemistry in the sedimentary environments of Kibiro, Panyimur, and Öxarfjörður. Reports 2013, no 12. UNU Geothermal Training Programme, United Nations University, Iceland, pp 201–234. <http://hdl.handle.net/10802/7417>
- Lee Davisson M, Criss RE (1996) Na–Ca–Cl relations in basinal fluids. *Geochim Cosmochim Acta* 60(15):2743–2752. [https://doi.org/10.1016/0016-7037\(96\)00143-3](https://doi.org/10.1016/0016-7037(96)00143-3)
- Li P, Wu J (2019) Sustainable living with risks: meeting the challenges. *Human Ecol Risk Assess* 25(1–2):1–10. <https://doi.org/10.1080/10807039.2019.1584030>
- Li P, Qian H, Wu J, Zhang Y, Zhang H (2013) Major ion chemistry of shallow groundwater in the Dongsheng Coalfield, Ordos Basin, China. *Mine Water and the Environment* 32(3):195–206. <https://doi.org/10.1007/s10230-013-0234-8>
- Li P, Wu J, Qian H (2014a) Hydrogeochemistry and quality assessment of shallow groundwater in the southern part of the Yellow River Alluvial Plain (Zhongwei Section), China. *Earth Sci Res J* 18(1):27–38. <https://doi.org/10.15446/esrj.v18n1.34048>
- Li P, Qian H, Wu J, Chen J, Zhang Y, Zhang H (2014b) Occurrence and hydrogeochemistry of fluoride in shallow alluvial aquifer of Weihe River, China. *Environ Earth Sci* 71(7):3133–3145. <https://doi.org/10.1007/s12665-013-2691-6>
- Li PY, Li XY, Meng XY, Li MN, Zhang YT (2016a) Appraising groundwater quality and health risks from contamination in a semiarid region of Northwest China. *Expo Health* 8(3):361–379. <https://doi.org/10.1007/s12403-016-0205-y>
- Li PY, Zhang YT, Yang NA, Jing LJ, Yu PY (2016b) Major ion chemistry and quality assessment of groundwater in and around a mountainous tourist town of China. *Expo Health* 8(2):239–252. <https://doi.org/10.1007/s12403-016-0198-6>
- Li P, Wu J, Qian H, Zhang Y, Yang N, Jing L, Yu P (2016c) Hydrogeochemical characterization of groundwater in and around a wastewater irrigated forest in the southeastern edge of the Tengger Desert, Northwest China. *Expo Health* 8(3):331–348. <https://doi.org/10.1007/s12403-016-0193-y>
- Li P, Tian R, Xue C, Wu J (2017) Progress, opportunities and key fields for groundwater quality research under the impacts of human activities in China with a special focus on western China. *Environ Sci Pollut Res* 24(15):13224–13234. <https://doi.org/10.1007/s11356-017-8753-7>
- Li P, Qian H, Wu J (2018a) Conjunctive use of groundwater and surface water to reduce soil salinization in the Yinchuan Plain, Northwest China. *Int J Water Resour Dev* 34(3):337–353. <https://doi.org/10.1080/07900627.2018.1443059>
- Li P, He S, He X, Tian R (2018b) Seasonal hydrochemical characterization and groundwater quality delineation based on matter element extension analysis in a paper wastewater irrigation area, northwest China. *Expo Health* 10(4):241–258. <https://doi.org/10.1007/s12403-17-0258-6>
- Li P, He S, Yang N, Xiang G (2018c) Groundwater quality assessment for domestic and agricultural purposes in Yan'an City, northwest China: implications to sustainable groundwater quality management on the Loess Plateau. *Environ Earth Sci* 77(23):775. <https://doi.org/10.1007/s12665-2018-7968-3>
- Li P, Wu J, Tian R, He S, He X, Xue C, Zhang K (2018d) Geochemistry, hydraulic connectivity and quality appraisal of multilayered groundwater in the Hongdunzi Coal Mine, Northwest China. *Mine Water Environ* 37(2):222–237. <https://doi.org/10.1007/s10230-017-0507-8>
- Li P, Tian R, Liu R (2019a) Solute geochemistry and multivariate analysis of water quality in the Guohua Phosphorite Mine, Guizhou Province, China. *Expo Health* 11(2):81–94. <https://doi.org/10.1007/s12403-018-0277-y>
- Li P, He X, Guo W (2019b) Spatial groundwater quality and potential health risks due to nitrate ingestion through drinking water: a case study in Yan'an City on the Loess Plateau of northwest China. *Human Ecol Risk Assess* 25(1–2):11–31. <https://doi.org/10.1080/10807039.2018.1553612>
- Ma ZY, Li XC, Zheng HJ, Li JB, Pei B, Guo S, Zhang XL (2017) Origin and classification of geothermal water from Guanzhong Basin, NW China: geochemical and isotopic approach. *J Earth Sci* 28(4):719–728. <https://doi.org/10.1007/s12583-016-0637-0>
- Morey GW, Fournier RO, Rowe JJ (1962) The solubility of quartz in water in the temperature interval from 25° to 300° C. *Geochimica et Cosmochimica Acta* 26(10):1029–1043
- Mu GX, Li F, Yan WZ, Li C, Jin HF, Liu F, Liu JQ, Zhao ZQ, Chen JP, Jin G, Ma ZY, Yang YY, Song QL, Li YC, Zhang PD, Gao L, Wang K, Yan XL, Wang XA (2016) Occurrence law of geothermal resources and key technologies for development and utilization in Guanzhong Basin. Geological Publishing House, Beijing (in Chinese)
- Pinti DL, Castro MC, Lopez-Hernandez A, Han G, Shouakar-Stash O, Hall CM, Ramírez-Montes M (2017) Fluid circulation and reservoir conditions of the Los Humeros Geothermal Field (LHGF), Mexico, as revealed by a noble gas survey. *J Volcanol*

- Geoth Res 333–334:104–115. <https://doi.org/10.1016/j.jvolgeores.2017.01.015>
- Qian H, Li PY (2011) Hydrochemical characteristics of groundwater in Yinchuan plain and their control factors. *Asian J Chem* 23:2927–2938
- Qian H, Li P, Wu J, Zhou Y (2013) Isotopic characteristics of precipitation, surface and ground waters in the Yinchuan Plain, Northwest China. *Environ Earth Sci* 70(1):57–70. <https://doi.org/10.1007/s12665-012-2103-3>
- Qian H, Wu J, Zhou Y, Li P (2014) Stable oxygen and hydrogen isotopes as indicators of lake water recharge and evaporation in the lakes of the Yinchuan Plain. *Hydrol Process* 28:3554–3562. <https://doi.org/10.1002/hyp.9915>
- Qin DJ, Pang ZH, Turner JV, Wen XR, Zhao YD, Xu XL, Liu T (2005a) Isotopes of geothermal water in Xi'an area and implication on its relation to karstic groundwater in North Mountains. *Acta Petrol Sinica*. <https://doi.org/10.3321/j.issn:1000-0569.2005.05.021> (in Chinese)
- Qin DJ, Turner JV, Pang ZH (2005b) Hydrogeochemistry and groundwater circulation in the Xi'an geothermal field, China. *Geothermics* 34(4):471–494. <https://doi.org/10.1016/j.geothermics.2005.06.004>
- Russak A, Sivan O (2010) Hydrogeochemical tool to identify salinization or freshening of coastal aquifers determined from combined field work, experiments, and modeling. *Environ Sci Technol* 44(11):4096–4102. <https://doi.org/10.1021/es1003439>
- Sanliyüksel D, Baba A (2011) Hydrogeochemical and isotopic composition of a low-temperature geothermal source in northwest Turkey: case study of Kirkgecit geothermal area. *Environ Earth Sci* 62(3):529–540. <https://doi.org/10.1007/s12665-010-0545-z>
- Su Y (2008) Study of isotopic and hydrochemical features of geothermal waters in the central Guanzhong Basin. MS thesis, Chang'an University, Xi'an, China (in Chinese)
- Wang S, Pang Z, Liu J, Lin P, Liu S, Yin M (2013) Origin and evolution characteristics of geothermal water in the Niutuozhen geothermal field, North China Plain. *J Earth Sci* 24(6):891–902. <https://doi.org/10.1007/s12583-013-0390-6>
- Wu J, Sun Z (2016) Evaluation of shallow groundwater contamination and associated human health risk in an alluvial plain impacted by agricultural and industrial activities, mid-west China. *Expo Health* 8(3):311–329. <https://doi.org/10.1007/s12403-015-0170-x>
- Wu J, Li P, Qian H, Duan Z, Zhang X (2014) Using correlation and multivariate statistical analysis to identify hydrogeochemical processes affecting the major ion chemistry of waters: case study in Laoheba phosphorite mine in Sichuan, China. *Arab J Geosci* 7(10):3973–3982. <https://doi.org/10.1007/s12517-013-1057-4>
- Wu J, Li P, Wang D, Ren X, Wei M (2019) Statistical and multivariate statistical techniques to trace the sources and affecting factors of groundwater pollution in a rapidly growing city on the Chinese Loess Plateau. *Human Ecol Risk Assess*. <https://doi.org/10.1080/10807039.2019.1594156>
- Xu GF (2014) Isotope and hydrochemical evidence of genetic about deep geothermal water-as the central of Guanzhong basin for an example. MS thesis Chang'an University, Xi'an, China (in Chinese)
- Xu P, Li M, Qian H, Zhang Q, Liu F, Hou K (2019) Hydrochemistry and geothermometry of geothermal water in the central Guanzhong Basin, China: a case study in Xi'an. *Environ Earth Sci* 78(3):87. <https://doi.org/10.1007/s12665-019-8099-1>
- Zhang XL (2016) The characteristics of isotopes and hydrogeochemistry for geothermal water in the piedmont of Qinling Mountain, as Tangyu town in Lantian county for an example. MS thesis, Chang'an University, Xi'an, China (in Chinese)
- Zhang XD, Qian H, Chen J, Qiao L (2014) Assessment of groundwater chemistry and status in a heavily used semi-arid region with multivariate statistical analysis. *Water* 6(8):2212–2232. <https://doi.org/10.3390/w6082212>
- Zhang X, Guo Q, Liu M, Luo J, Yin Z, Zhang C, Zhu M, Guo W, Li J, Zhou C (2016) Hydrogeochemical processes occurring in the hydrothermal systems of the Gonghe-Guide basin, northwestern China: critical insights from a principal components analysis (PCA). *Environ Earth Sci* 75(16):1187. <https://doi.org/10.1007/s12665-016-5991-9>
- Zhang Y, Wu J, Xu B (2018) Human health risk assessment of groundwater nitrogen pollution in Jinghui canal irrigation area of the loess region, northwest China. *Environ Earth Sci* 77(7):273. <https://doi.org/10.1007/s12665-018-7456-9>
- Zhao H (2009) Study on hydrogeochemistry and environmental impacts from exploitation and utilization of geothermal water in Guanzhong Basin. DS thesis, Chang'an University, Xi'an, China (in Chinese)
- Zhu C, Hu S, Qiu N, Jiang Q, Rao S, Liu S (2018) Geothermal constraints on Emeishan mantle plume magmatism: paleotemperature reconstruction of the Sichuan Basin, SW China. *Int J Earth Sci* 107(1):71–88. <https://doi.org/10.1007/s00531-016-1404-2>

Publisher's Note Springer Nature remains neutral with regard to jurisdictional claims in published maps and institutional affiliations.